Enhanced recrystallization and dopant activation of P^+ ion-implanted super-thin Ge layers by RF hydrogen plasma treatment

Alexei N. Nazarov, Volodymyr O. Yukhymchuk, Yurii V. Gomeniuk, Sergiy B. Kryvyi, Pavel N. Okholin, Petro M. Lytvyn, Vasyl P. Kladko, and Volodymyr S. LysenkoVolodymyr I. GlotovIllya E. GolentusEnrico NapolitaniRay Duffy

Citation: Journal of Vacuum Science & Technology B, Nanotechnology and Microelectronics: Materials, Processing, Measurement, and Phenomena **35**, 051203 (2017); doi: 10.1116/1.4996139

View online: http://dx.doi.org/10.1116/1.4996139

View Table of Contents: http://avs.scitation.org/toc/jvb/35/5

Published by the American Vacuum Society

Enhanced recrystallization and dopant activation of P^+ ion-implanted super-thin Ge layers by RF hydrogen plasma treatment

Alexei N. Nazarov,[a] Volodymyr O. Yukhymchuk, Yurii V. Gomeniuk, Sergiy B. Kryvyi, Pavel N. Okholin, Petro M. Lytvyn, Vasyl P. Kladko, and Volodymyr S. Lysenko
Lashkaryov Institute of Semiconductor Physics NAS of Ukraine, 41 Nauky pr., 03680 Kyiv, Ukraine

Volodymyr I. Glotov
Research Institute of Microdevices NAS of Ukraine, 3, Pivnychno-Syretska Str., 04130 Kyiv, Ukraine

Illya E. Golentus
Kurdyumov Institute of Physics of Metalls NAS of Ukraine, 36 Vernadskiy blvd., 02000 Kyiv, Ukraine

Enrico Napolitani
Dipartimento di Fisica e Astronomia, Università di Padova and CNR-IMM Matis, via Marzolo 8, 35131 Padova, Italy

Ray Duffy
Tyndall National Institute, University College Cork, Cork T12 R5CP, Ireland

(Received 22 April 2017; accepted 11 July 2017; published 1 August 2017)

Radio-frequency (RF) hydrogen plasma treatment, thermal annealing in a furnace, and rapid thermal annealing of high-dose P^+ ion implanted p-type Ge layers have been studied by Raman scattering spectroscopy, atomic force microscopy, secondary ion mass spectrometry, electrochemical capacitance–voltage profiling, four-point probes method, and x-ray reflectometry. It was shown that low-temperature RF plasma treatment at temperature about 200 °C resulted in full recrystallization of amorphous Ge layer implanted by P^+ ions and activation of implanted impurity up to $6.5 \times 10^{19}\,cm^{-3}$ with a maximum concentration at the depth of about 20 nm. Rapid thermal annealing (15 s) and thermal annealing (10 min) in nitrogen ambient required considerably higher temperatures for the recrystallization and activation processes that resulted in diffusion of implanted impurity inside the Ge bulk. It was demonstrated that RF plasma treatment from the samples with front (implanted) side resulted in considerable stronger effects of recrystallization and activation as compared with the same treatment from the back (unimplanted) side. The experiment shows that nonthermal processes play an important role in enhanced recrystallization and dopant activation during the RF plasma treatment. Mechanisms of enhanced modification of the subsurface implanted Ge layer under plasma treatment are analyzed. © *2017 American Vacuum Society*.
[http://dx.doi.org/10.1116/1.4996139]

I. INTRODUCTION

According to the review paper,[1] equipment for plasma etching of the semiconductor and dielectric wafers can be employed for RF hydrogen plasma treatment (RFPT) which is a very promising method for modification of thin surface semiconductor and dielectric layers and also of thin layers of nanostructured materials. In papers 2–4, it was demonstrated that defects and dopant in implanted silicon subsurface layers can be effectively annealed and activated correspondingly at low temperature by RF hydrogen plasma treatment. However, in the case of the high-dose ion implanted Si layers, when the amorphous subsurface layer is formed, low-temperature RFPT does not lead to the recrystallization of the amorphous Si subsurface layer but creates the completely mechanically relaxed amorphous layer.[5] Due to considerably lower recrystallization temperature of amorphous Ge layers as compared to amorphous Si layers,[6] and to the fact that RF plasma treatment anneals the defects within a thin surface layer,[1] it should be expected that RFPT could be successfully applied to crystallize thin amorphous Ge layer and activate the implanted dopant to form shallow p-n junctions. In the Okholin's paper,[7] it was shown that thin amorphous implanted Ge layer can be recrystallized by RFPT, but comparison with the standard thermal annealing (TA) has not been performed and possibility of a dopant activation for shallow n^+/p junction formation has not been studied. Therefore, the presented work provides a careful comparison of recrystallization of implanted amorphous super-thin Ge layer by RFPT with TA and studying of the implanted dopant activation in thin Ge layer. Additionally, a set of experiments were performed to reveal the nonthermal factors that can enhance recrystallization and dopant activation and change the Ge surface properties.

II. EXPERIMENT

A. Samples

The monocrystalline germanium (Ge) wafers with ⟨100⟩ orientation were fabricated by liquid encapsulated Czochralski method and were polished on the front side. The p-type Ge wafer with carriers' concentration of about $(7 \pm 2) \times 10^{16}\,cm^{-3}$ was implanted by P^+ ions with the

[a]Electronic mail: nazarov@lab15.kiev.ua

energy 12 keV and the dose of 1×10^{15} ions/cm^2. As it was determined from the ion distribution profile simulation by the stopping and range of ion in matter (SRIM) code, a maximum of the profile was situated about 15 nm from the Ge surface.

RF plasma treatment (13.56 MHz) was performed in a diode type reactor[1] in the forming gas (90% N_2 + 10% H_2), nitrogen and hydrogen atmosphere. The samples were located on the additional heated (up to 200 °C) RF electrode, and RF plasma treatment was performed from the side of implanted layer. Some samples were treated face-down to extract clearly nonthermal effects. The RF plasma power density was varied from 0.5 to 2.0 W/cm^2, and the treatment duration was 10 min. The sample temperature for plasma treatment was monitored *in situ* using specially calibrated thermal paints that were deposited on the back side of the samples. The results of the measurements have been presented in the paper.[8] Control TA was carried out in a standard furnace in nitrogen ambient in the temperature range from 150 to 400 °C for 10 min. A part of the implanted Ge samples was annealed by rapid thermal annealing (RTA) method in the temperature range from 350 to 550 °C during 15 s in nitrogen ambient. All treatments were performed without etching of the surface layer.

B. Methods of measurements

The phase composition of the samples was studied by Raman scattering spectroscopy (RSS) at room temperature. Additionally, as it was demonstrated in papers 9–11, the RSS allows us to estimate the degree of incorporation (activation) of the implanted dopant (phosphorus in our case) in the crystalline Ge lattice. For this, the local phonons of phosphorus atoms in the crystalline Ge lattice (~345–350 cm^{-1}) were studied. The RS spectra were studied using a double monochromator equipped with Andor CCD camera. YAG laser ($\lambda = 532$ nm, $P < 10$ mW) was used for excitation. The surface morphology was studied by atomic force microscopy (AFM) using NanoScope IIIa Dimension 3000.

The thickness and composition of the implanted layer was analyzed with a SIMS CAMECA IMS-4f spectrometer using an O_2^+ 3 keV and 200 nA primary beam rastered over an area of $250 \times 250\ \mu m^2$ while collecting $^{31}P^{16}O^+$ secondary ion from a central area with 150 μm diameter. The profile of activated implanted impurity was obtained by electrochemical capacitance–voltage profiling (ECV).[12] The surface sheet resistance (R_{sh}) and the estimation of doping concentration in the implanted layer were performed by four-point probes (4PP) method.[13]

The density of subsurface Ge layer before and after the treatments was studied by x-ray reflectometry (XRR)[14] using PANalytical X'Pert Pro MRD XL diffractometer (X'Pert, PANalytical B.V., Almelo) with a fourfold (220) Ge monochromator and 0.1 × 10 mm incident beam collimator. The diffracted beam was collimated by a parallel plate collimator with the acceptance angle of 0.27°, used in combination with a 0.1 mm receiving slit. The method of density profile simulation from experimental data is presented in the Appendix.

III. RESULTS AND DISCUSSION

A. Recrystallization of the amorphous layer: Raman scattering study

1. Thermal annealing

The RS spectra of the as-implanted and thermally annealed p-Ge samples are presented, respectively, in Figs. 1(b) and 1(a), respectively. The P^+ implanted sample showed a wide peak with maximum at 273 cm^{-1} related to the amorphous Ge phase and a narrow asymmetric peak at 301 cm^{-1} with half-width (Γ) about 4.7 cm^{-1} which is ascribed to the crystalline Ge phase. In our case, the amorphous Ge layer has a thickness of about 20 nm (according to the SRIM simulation), and the penetration depth for the light with the wavelength of 532 nm is about 10 nm. Asymmetry of the crystalline component peak can be caused by Raman scattering of Ge nanocrystals[15] and stretched Ge layer.[16] Besides, the half-width of the peak at 300 cm^{-1} is relatively small even after the ion implantation, which is an evidence of the absence of big stresses and the formation of very small nanocrystallites. After TA at 150 °C, the spectrum consist of

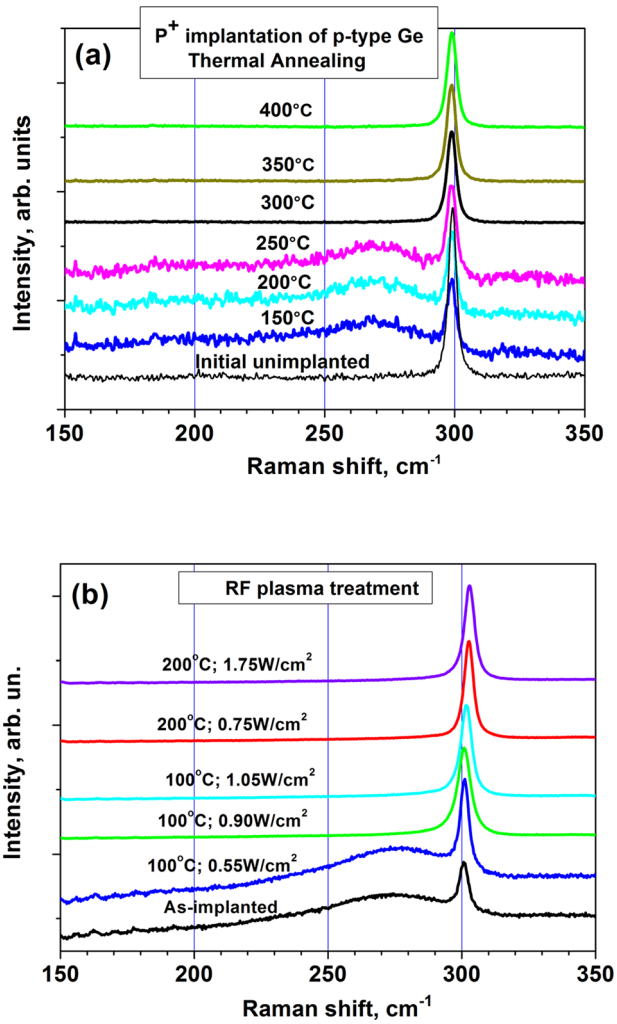

FIG. 1. (Color online) Normalized RS spectra for P^+ ions implanted p-Ge: (a) thermal annealed at nitrogen atmosphere for 10 min; (b) treated by RF plasma in forming gas (10%H_2 + 90%N_2) for 10 min.

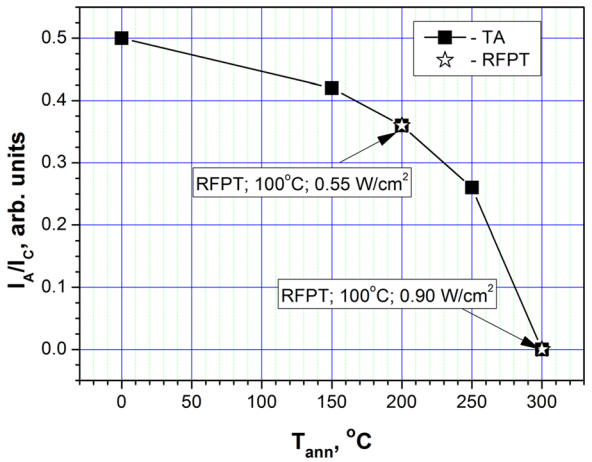

FIG. 2. (Color online) Dependence of I_A/I_C vs temperature of TA and for RFPT for RS spectra of P^+ ions implanted p-Ge.

a wide peak with a maximum at 273 cm^{-1} and a narrow asymmetric peak at 298.8 cm^{-1} with half-width (Γ) of about 4.7 cm^{-1}. The increase in annealing temperature leads to the decrease in the intensity of the wide peak (amorphous phase, I_A) and to the increase in the intensity of the narrow peaks (crystalline phase, I_C) (see Fig. 2). The TA at 300 °C results in the complete crystallization of the amorphous phase in the Ge thin layer [Fig. 1(a)]. At increasing temperature of TA process, the shift of the "crystalline" peak has not been observed, and the half-width of the peak decreases up to 4.3 cm^{-1}. The decrease in half-width of the peak of the Ge crystalline phase is caused by decreasing quantity of structural defects, which causes the prolongation of phonons lifespan ($\Gamma \sim 1/\tau_{phon}$). Figure 1(a) shows that a further increase in annealing temperature of the samples to 400 °C did not change the parameters of the peak.

2. RF plasma treatment

RF plasma treatment of the implanted Ge leads to crystallization of the implanted surface layer at considerably lower temperature than in the case of TA. At 100 °C of the sample holders and the power density at 0.9 W/cm^2, the thin implanted amorphous layer is completely crystallized [Fig. 1(b)]. The actual temperature of the samples in this case is about 160 °C,[8] but the effect of recrystallization of the surface implanted amorphous layer corresponds to 300 °C of TA. Using the amplitude ratio of integral intensities of TO-band for the amorphous phase and the band of the crystal phase $I_A/I_C = 0.36$ at 100 °C and power density 0.55 W/cm^2, it is possible to estimate the efficiency of the RFPT in comparison with TA. Such process results in thermal heating of the sample for about 120 °C,[8] but it has an efficiency of amorphous layer recrystallization corresponding to TA at 200 °C (see Fig. 2). The increase in the RF power density (note that the sample was additionally heated up to 200 °C) resulted in the reduction of the crystalline peak half-width that is related to the decrease of defect concentration in the implanted layer. RF plasma treatment strongly affects only the thin surface layer of the semiconductor, so it is natural to assume (as in RTA) the reduction of tensile stresses (annealing thin surface layer) in the samples with the increase in RF plasma power, which leads to the high-frequency shift of the crystalline peak [Fig. 1(b)].

B. Dopant activation

1. Raman scattering study

Another important feature of the Raman spectroscopy is a possibility of estimating the dopant impurity incorporation into the sites of the crystalline lattice. For the case of P^+ ion implantation in p-Ge emergence and the intensity of Raman band in the range of 345–350 cm^{-1} which corresponds to the mode of local vibrations related to phosphorus atoms localized in sites of crystalline Ge lattice.[11] These local vibrations can be observed only in the case of fully recrystallized implanted layer. Figure 3(a) shows Raman spectra in the spectral range of phosphorus local vibrations before and after thermal annealing. In the as-implanted samples [Fig. 1(b)], the subsurface layer consists of amorphous and nanocrystalline phases. So, the phosphorus local vibrations are not observed in the spectrum. After thermal annealing in nitrogen atmosphere for 10 min at 300 and 400 °C, the

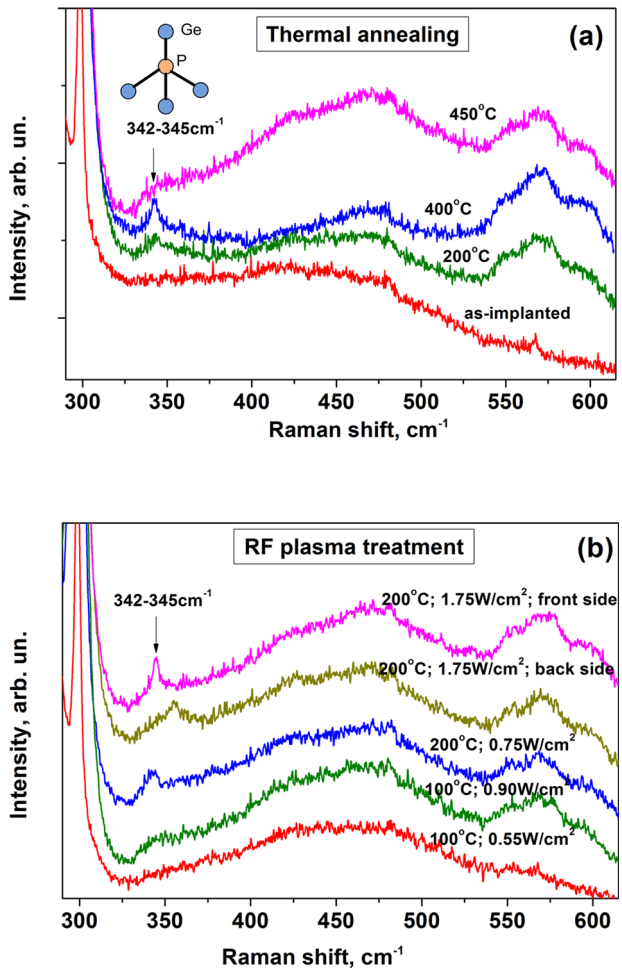

FIG. 3. (Color online) Raman spectra in the range of local phonon of implanted p-Ge: (a) after thermal annealing in nitrogen atmosphere; (b) after RF plasma treatment in forming gas.

Raman peak at 342 cm^{-1} associated with local vibrations of P incorporated into Ge crystalline lattice is generated. Annealing at 450 °C results also in total recrystallization of the amorphous implanted layer; however, intensive Raman band relating to phosphorus local vibrations is not observed. This effect can be linked with strong redistribution of phosphorus atoms in bulk of Ge that can result in essential decrease of the Raman band intensity.

Figure 1(b) shows that RF plasma treatment at the temperature of 100 °C and the power density of 0.90 W/cm^2 results in recrystallization of the amorphous implanted layer. In this case, in the range of phosphorus local vibrations, a weakly pronounced Raman band in the range of 345–350 cm^{-1} is formed [Fig. 3(b)], associated with phosphorus incorporation into sites of the Ge lattice. The increase in additional heating temperature of the plasma treatment up to 200 °C even at a lower power density (0.75 W/cm^2) results in the increase of phosphorus local phonon intensity [Fig. 3(b)] although a half-width of the crystalline line of Ge in Raman spectrum [Fig. 2(b)] remains large enough ($\Gamma = 5.7\ cm^{-1}$) that is associated with defectiveness of the subsurface layer. A further increase in the power density up to 1.75 W/cm^2 decreases the half-width of the crystalline line up to 4 cm^{-1} and considerably increases the phosphorus incorporation into sites of the Ge lattice [Fig. 3(b)].

2. SIMS and ECV Profiling

The study of phosphorus distribution and activated impurity distribution in P^+-implanted p-Ge was performed correspondingly by SIMS and ECV. It was shown that RF plasma treatment in forming gas at 1.5 W/cm^2 and additional heating at 200 °C results in the same phosphorus atom distribution as in the case of the as-implanted material [Fig. 4(a)]. The only difference observed in the 10 nm thickness surface layer of the RF treated samples is that the SIMS measurements show an increased concentration of phosphorus atoms. The observed effect is a measurement artifact that can be associated with the surface destruction by plasma treatment, which is observed by AFM technique[7] and XRR method. The distribution of the phosphorus atoms, which was obtained after RTA at 450 °C for 15 s, shows considerable spreading of the phosphorus profile into the sample depth.

Figure 4(b) demonstrates the distribution of activated impurity in the subsurface layer of p-Ge after RF plasma treatment and RTA. The observed profiles are very similar to those measured by SIMS technique. However, the concentration of activated impurity is considerably less than the concentration of the implanted phosphorus atoms and corresponds to 20% of the implanted phosphorus concentration at the depth of 20 nm from the surface, both for RF and RT annealing. At the same time, the activated phosphorus concentration at this depth is 6.5×10^{19} atoms/cm^3 for the RF plasma treatment and $(2–3) \times 10^{19}$ atoms/cm^3 for the RTA. Thus, RF plasma treatment forms a narrow profile of implanted phosphorus with the high concentration of activated dopant near the Ge surface that confirms low temperature of the treatment and enhanced activation process.

3. Surface sheet resistance study

Figure 5 shows surface sheet resistances measured by 4PP method for the implanted Ge layers after RFPT, TA, and RTA. It should be noted that TA in nitrogen ambient at the temperature of about 400 °C demonstrates significantly higher sheet resistance than RFPT even at 0.75 W/cm^2 with additional heating at 200 °C. Such RFPT regime corresponds to the total thermal heating of the sample to approximately 250 °C.[8] A further increase in the RFP treatment power results in a decrease of the sheet resistance which reaches 65 Ω/sq (see Fig. 5) that corresponds to the maximum of activated dopant concentration of about $6 \times 10^{19}\ cm^{-3}$ (as it was shown in the previous section). Knowing the values of the sheet resistance and the corresponding free carrier concentration in the subsurface layer, and using the relation between the resistivity and carrier concentration according to Cuttriss,[17] it is possible to roughly estimate the thickness of the n^+-layer of the n^+/p junction. In our case, for the samples treated with RFP, the thickness is about 100 nm. This value roughly corresponds to the thickness of the layer where the free carrier concentration in n^+ layer equals to $1 \times 10^{17}\ cm^{-3}$ (a dopant concentration of the Ge wafer). The

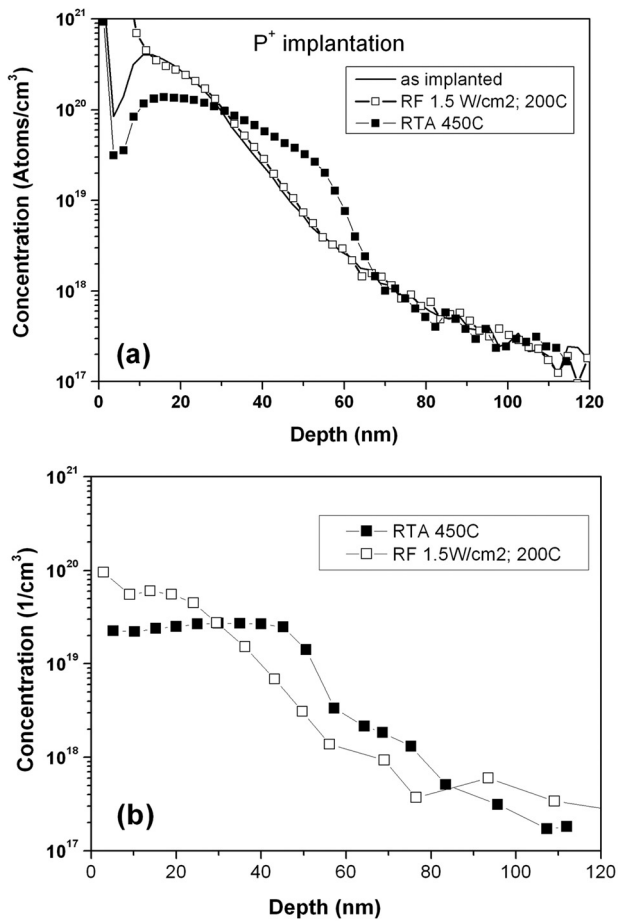

FIG. 4. Distribution of the implanted impurity after P^+-ion implantation of p-Ge with energy of 12 keV and dose of 1×10^{15} ions/cm^2 measured by SIMS techniques (a) and distribution of electrical active impurity measured by ECV technique (b): ——, as implanted; □, treated in RF plasma (1.5 W/cm^2; 200 °C, for 10 min); and ■, RTA (450 °C for 15 s).

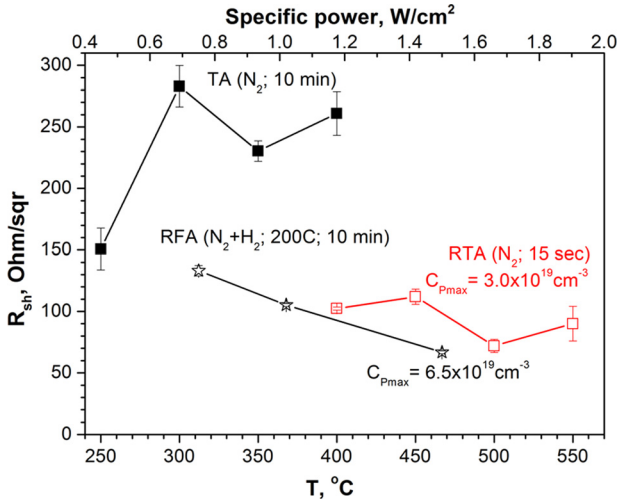

FIG. 5. (Color online) Surface sheet resistance for thermal annealed, RF plasma and RT treated of P^+-ion implanted p-Ge.

same thickness of the surface high doped layer is obtained for RTA samples with the activated dopant concentration equal to 3×10^{19} cm^{-3}. Using this value of n^+ layer thickness and the sheet resistance (about 250 Ω/sq) for TA at 400 °C presented in Fig. 5, it is possible to estimate the activated dopant concentration for this case which is equaled to about 6×10^{18} cm^{-3}. Because the maximum temperature of the sample heating at employed RFPT ($W = 1.50$ W/cm^2; additional heating—200 °C) is about 350 °C,[8] we can conclude that the RFPT is significantly more effective for phosphorus doping impurity activation than TA.

C. Nonthermal effects at RF plasma treatment

1. Effect of electron and ion bombardment

According to Nazarov's review paper,[1] during RF plasma treatment, the front side of the implanted samples can be affected by the following factors: low-energy electron and ion bombardment; temperature; UV and soft x-ray irradiation; alternating electric field, proton injection from plasma.

The low-energy electron and ion bombardment can result in destruction of the thin surface layer that can be shown from AFM experiments (Fig. 6). If the initial samples of p-type Ge implanted by P^+ ions have a root mean square (RMS) surface roughness equals to 226 pm [Fig. 6(a)], the RF plasma treatment at $T = 100$ °C and $P = 1.25$ W/cm^2 changes a surface morphology leading to RMS surface roughness of 361 pm [Fig. 6(b)]. In the latter case, we observed the nanostructured surface composed of knolls with the base sizes ranging from 20 to 8 nm and heights of about 1.0 nm. Thus, the low-energy electron and ion bombardment slightly affects the subsurface properties of the Ge samples.

The SIMS experiments on the samples treated by RF hydrogen plasma have shown the presence of oxygen in the thin Ge layer (about 10 nm thickness). This effect can be associated with germanium oxide formation on the surface of the samples during the plasma treatment due to the presence of residual oxygen in the chamber. An XRR technique was used to study the structure of the thin subsurface Ge layer. This method allows us to extract the mass density of the material in the thin subsurface layer.

Figure 7(a) shows experimental and simulation data of x-ray reflectivity in dependence on an incident angle for several cases. The initial P^+ ion implanted sample demonstrates the appearance of a 4-nm thick thin layer on the Ge surface with variable mass density equal to 20% from the Ge mass density of the surface [Fig. 7(b)]. The simulation method is presented in the Appendix. The observed layer is probably associated with the existence of native germanium oxide on the Ge surface. It was shown[18] that the first oxide monolayer on the Ge surface appears at room temperature during first 15 s after placing the chemical etched sample in a clean room condition.

RF plasma treatment at 200 °C (power density of 1.75 W/cm^2) results in a strong decrease of reflectivity in the first kink and generation of large second kink in the x-ray reflectivity versus incident angle dependence which is associated with the additional layer formation under the first layer [Fig. 7(a)]. The simulation shows that the surface layer is denser than the initial one, and the deep layer is even denser than the surface one [Fig. 7(b)]. The second layer is located at the depth of up to 10 nm. It should be noted that second layer formation is associated more with the density of RF plasma

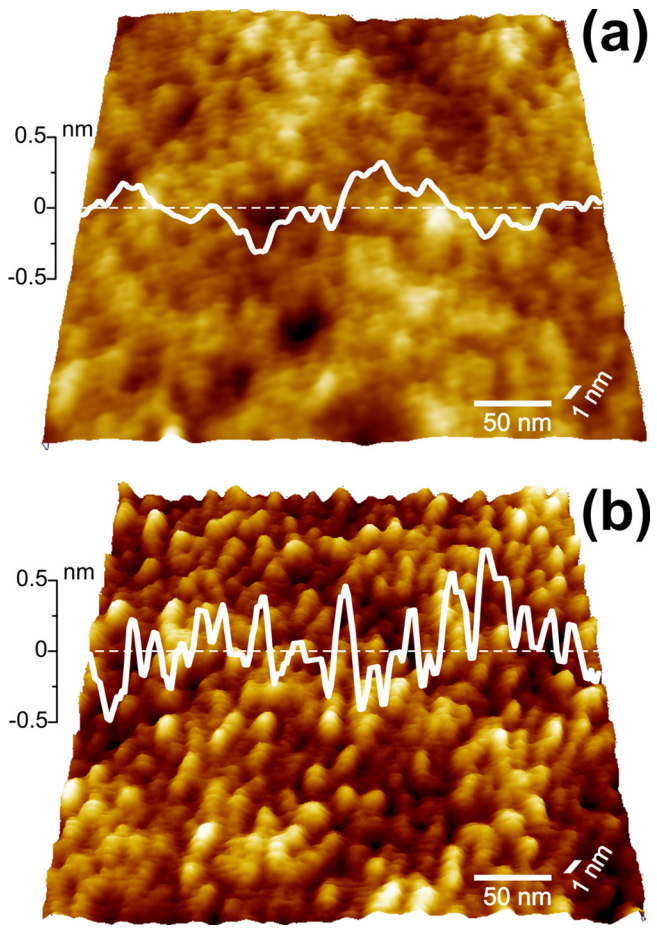

FIG. 6. (Color online) 3D AFM images of the as implanted p-Ge (a) and the sample after RF plasma treatment ($T = 100$ °C and $P = 1.25$ W/cm^2) (b). Corresponding profiles of the surface relief along dashed lines are shown in insets.

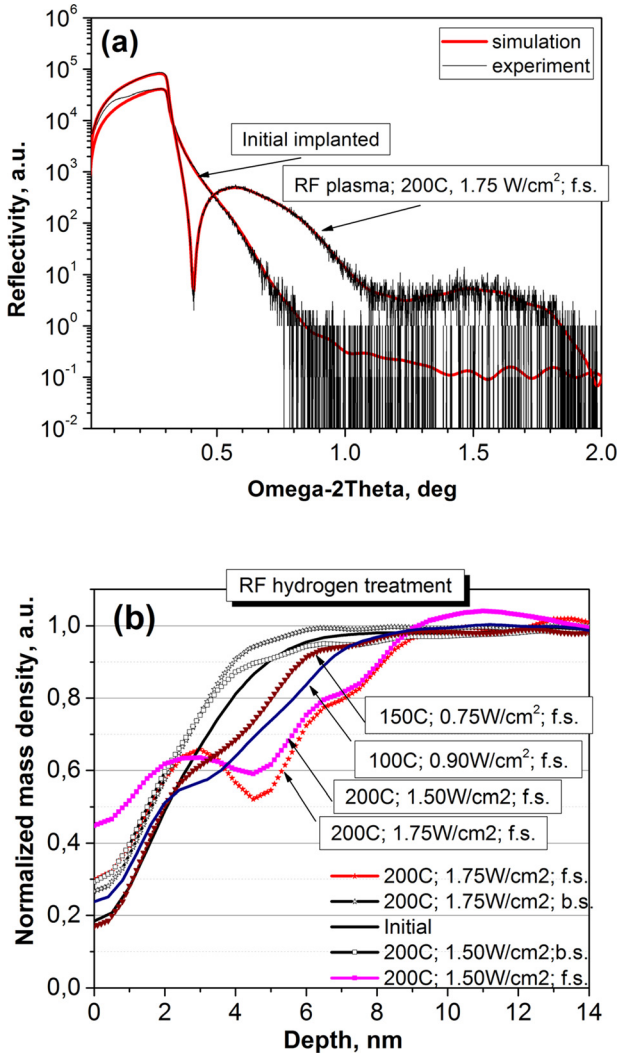

FIG. 7. (Color online) Examples of x-ray reflectivity curves vs incident angle and their simulation (a) and calculated curves of mass density mass density normalized to the bulk mass density of the crystalline Ge vs depth for RF plasma treated implanted samples (b).

power than with the temperature of the treatment. The treatment from unimplanted side of the sample (back side) leads to minor changes in mass density of the surface layer. Under such treatment, the implanted Ge layer is subjected to heating temperature mainly but not to electron and ion bombardment, light emission, and ionized hydrogen and nitrogen. Thus, one can conclude that under RF hydrogen plasma treatment, the thin surface layer is transformed to a dense layer probably associated with germanium oxide or germanium oxynitride. The SIMS measurements confirm this conclusion demonstrating enhanced oxygen concentration in this thin surface region. However, the main dose of implanted ions is located deeper than this shallow oxide layer, and its formation does not affect the distribution of the activated implanted impurity.

2. Extraction of nonthermal factors effecting on the implanted layer

Main effects which can enhance the ordering and crystallization of our amorphous layers are light irradiation with the combination of alternating electric field and protons as catalyst of defect transformation. Under RF plasma treatment from the back side, the main factors that influence the implanted layer are temperature, soft x-ray irradiation, and alternating electric field. To distinguish nonthermal factors which can lead to a reduction of the crystallization temperature and temperature of dopant activation of the implanted Ge samples, experiments with the treatment of the samples by RF plasma discharge from the implanted (front) side and the back side in the same technological process were carried out [see inset in Fig. 8(a)]. Figure 8(a) demonstrates that RF treatment of the P^+-implanted side of p-Ge results in enhanced crystallization of the amorphous implanted layer (disappearance of wide RS peak at 273 cm^{-1} of amorphous phase). RF plasma treatment of the back side of the samples shows a considerable effect on thin amorphous layer but not the complete recrystallization. It should be noted that recrystallization of P^+-implanted amorphous layer takes place after annealing at 300 °C for 10 min [Fig. 1(a)]. Thus, the temperature used for heating the sample was not higher than 250 °C at RF plasma treatment at the used regime (T = 200 °C, P = 1.55 W/cm^2). The comparison of local vibration modes of Raman measurements after front and back side RF plasma treatment demonstrated enhanced incorporation of phosphorus atoms into the sites of Ge lattice after the front side treatment [see Fig. 3(b)].

All RF plasma treatments presented before were performed in the mixture of gases 10% H_2 and 90% N_2. To understand a hydrogen effect on the RF annealing, the treatments in pure hydrogen and nitrogen were performed. Raman spectra for P^+-implanted p-Ge after such treatments are presented in Fig. 8(b). It can be seen that the RF plasma treatment in pure hydrogen atmosphere results in the considerably stronger effect of the amorphous layer recrystallization than in the case of the RF plasma treatment in pure nitrogen atmosphere. Thus, hydrogen can be affected strongly on enhanced annealing of the thin amorphous implanted layers. The model of vacancy defect annealing and enhanced dopant activation in implanted silicon was presented in papers 1, 19, and 20 This model uses catalytic properties of hydrogen which decrease the potential barrier for reaction of interstitial atom incorporation into hydrogenated vacancy site. In the case of germanium, the temperature of hydrogen diffusion is lower, and the bonding energy proton with a vacancy[21,22] is smaller than in the case of silicon that results in the decrease of recrystallization and activation temperatures. So, it can be suggested that the proposed mechanism of enhanced hydrogen annealing for silicon can take place in germanium.

However, in germanium, the light-stimulated processes of defect transformations[23] may take place also together with hydrogen stimulated ones. To extract the effect of light irradiation, the experiment of treatment the samples from front and back sides was performed in the case of RTA. It was shown that RTA from the front side is more effective that the treatment from the back side [Fig. 8(c)], which leads to enhanced recrystallization of the Ge amorphous layer and the activation of dopant impurity. It should be noted that

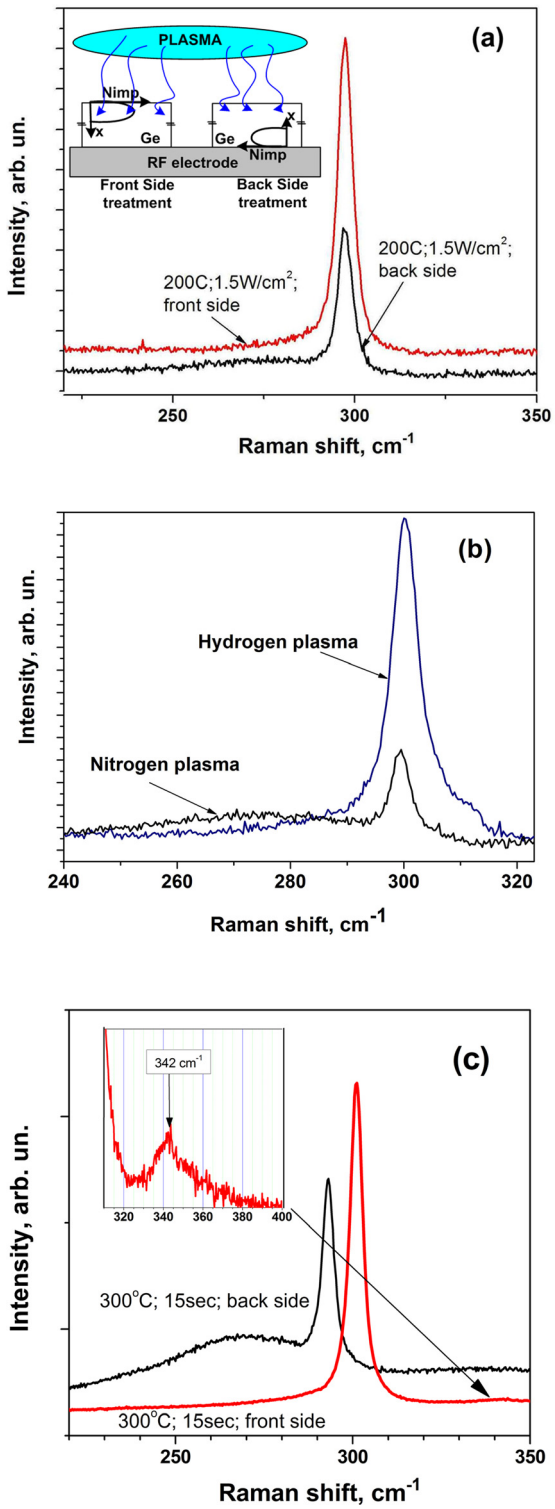

FIG. 8. (Color online) RS spectra for p-Ge implanted by P^+ ions: (a) treated by RF plasma in forming gas from front side and back side of the samples; (b) treated by RF plasma in hydrogen and nitrogen atmosphere; and (c) after RTA from front and back sides. Inset: RS spectrum for front side RTA in the range of local phonons.

heating of the germanium wafer with thickness of about 300 μm during 15 s results in uniform temperature distribution through the sample thickness. Thus, in case of implanted Ge light can also noticeably increase the effect of annealing of the implanted layer.

IV. CONCLUSIONS

Low-temperature RF plasma treatment of implanted germanium in forming gas allows us to recrystallize thin amorphous implanted Ge layers at temperature at least by 100 °C less than standard thermal annealing and RTA in nitrogen atmosphere, and the temperature of the sample heating at the plasma process does not exceed 200 °C. Distribution of the implanted impurity (such as phosphorus) after RF plasma annealing is not different from initial distribution of the implanted impurity. After RF plasma treatment, the concentration of activated phosphorus in shallow surface layer can reach 6×10^{19} atoms/cm^3 that is considerably higher than in the case of TA and RTA. Nonthermal factors such as proton injection, light and UV, and alternating electric field can play a significant role in the enhancement of the recrystallization and activation processes. Additionally, RF plasma treatment in forming gas synthesizes the thin dielectric layer with a total thickness not more than 10 nm.

APPENDIX

To obtain the profiles of electron density distribution, a simulation and further fit of the theoretical curve to the experimental results were used. The algorithm of the simulation is as follows:

(1) Setting depth L (of the order of 20–30 nm), within which a disturbance is probably focused, we divide this layer of the crystal thickness of L to N sublayers with a thickness of "d" (on the order of 0.3–0.5 nm).

(2) Susceptibility χ_n (where n = 1, 2,…, N) inside every sublayer is assumed to be constant, and behind the last sublayer, susceptibility is equaled to that of crystalline germanium: $\chi_N = \chi_{Ge}$. The set of N-1 parameters of χ_n is necessary to be calculated.

If the χ_n are known, the intensity of specular reflection on the multilayer system is calculated by the Parrata's formula[24]

$$R_{N+1} = 0,$$

$$R_{N-n+1} = \frac{\Psi_{N-n+1} + R_{N-n+2}}{1 + \Psi_{N-n+1} R_{N-n+2}} \exp(2ik_{N-n,z}d),\ 1 \le n \le N-1,$$

$$R_{theor} = R_1 = \frac{\Psi_1 + R_2}{1 + \Psi_1 R_2}.$$

Here, R_n is the reflection coefficient from the n-th layer, $k_{n,z} = K\sqrt{\alpha^2 + \chi_n}$—the z-component of the wave vector inside of n-th layer, α—the slip angle of the incident wave, and

$$\Psi_n = \frac{k_{n-1,z} - k_{n,z}}{k_{n-1,z} + k_{n,z}}.$$

Our task is to choose the values χ_n so that the difference between the experimental (preadjusted) and theoretical intensity is minimized. But, as it is known, the given

XRR curve can correspond to many oscillating susceptibility profiles. Thus, we will minimize the function

$$F = \sum_k \left(\lg R_{\exp}(\alpha_k) - \lg R_{theor}(\alpha_k)\right)^2 + \mu \sum_n (\chi_{n+1} - \chi_n)^2,$$

which allows us to determine best monotonous profile by selecting a proper value of μ as it was presented in paper 25. The minimum of the function is searched by using the "lsqnonlin" function in MATLAB softwere[4] which uses the Levenberg–Makuarda algorithm. To speed up the search process, the Jacobian function F is also explicitly calculated.

(3) If the calculation gives a constant value of the susceptibility profile in the middle of the crystal, the output value L should be increased, and the calculation has to be repeated.

If the adsorption and dispersion are neglected, using known ratio, from the susceptibility profiles, the electron density (ρ_{el}) and mass density (ρ_{m}) profiles can be found

$$|\chi_n| = \frac{\lambda^2 r_{el}}{\pi}\rho_{el}, \quad \rho_m = \frac{\rho_{el}A}{N_A Z}, \quad \text{and} \quad \rho_m = \frac{A\pi|\chi_n|}{N_A Z\lambda^2 r_{el}}.$$

Here, $r_{el} = e^2/4\pi\varepsilon_o m_o c^2 \approx 2.82 \times 10^{-15}(m)$ is the electron radius, Z is the atomic number, A is the mass number, $\lambda = 0.15405\,\mathrm{nm}$ ($\mathrm{CuK}_{\alpha 1}$) is the x-ray wavelength $\lambda = 0.15405\,\mathrm{nm}$ ($\mathrm{CuK}_{\alpha 1}$), and N_A is the Avogadro constant.

[1]A. N. Nazarov, V. S. Lysenko, and T. M. Nazarova, Semicond. Phys. Quantum Electron. Optoelectron. **11**, 101 (2008).
[2]V. S. Lysenko, A. N. Nazarov, S. A. Valiev, I. M. Zaritskii, T. E. Rudenko, and A. S. Tkachenko, Phys. Status Solidi A **113**, 653 (1989).
[3]A. N. Nazarov, V. S. Lysenko, S. A. Valiev, M. M. Lokshin, A. S. Tkachenko, and I. A. Kunitskii, Phys. Status Solidi A **120**, 447 (1990).
[4]M. Ya. Valakh, V. S. Lysenko, A. N. Nazarov, G. Yu. Rudko, A. S. Tkachenko, and N. I. Shakhraychuk, Res. Nucl. Instrum. Methods Phys., B **44**, 146 (1989).
[5]V. V. Artamonov, V. S. Lysenko, A. N. Nazarov, V. V. Strelchuk, M. Ya. Valakh, and I. M. Zaritskii, Semicond. Sci. Technol. **6**, 1 (1991).
[6]C. Claeys and E. Simoen, *Germanium-Based Technologies: From Materials to Device* (Elsevier, Oxford, Amsterdam, 2007).
[7]P. N. Okholin *et al.*, Mater. Sci. Semicond. Process. **42**, 204 (2016).
[8]A. N. Nazarov, V. I. Kilchytska, I. P. Barchuk, A. S. Tkachenko, and S. Ashok, J. Vac. Sci. Technol., B **18**, 1254 (2000).
[9]A. Sanson, E. Napolitani, G. Impellizzeri, M. Giarola, D. De Salvador, V. Privitera, F. Priolo, G. Mariotto, and A. Carnera, Thin Solid Films **541**, 76 (2013).
[10]A. Sanson, M. Giarola, E. Napolitani, G. Impellizzeri, V. Privitera, A. Carneraa, and G. Mariotto, J. Raman Spectrosc. **44**, 665 (2013).
[11]N. Fukata, K. Sato, M. Mitome, Y. Bando, T. Sekiguchi, M. Kirkham, J. Hong, Z. L. Wang, and R. L. Snyder, ASC Nano **4**, 3807 (2010).
[12]H. C. Mogul, A. J. Steckl, G. Webster, M. Pawlik, and S. Novak, Appl. Phys. Lett. **61**, 554 (1992).
[13]D. K. Schroder, *Semiconductor Material and Device Characterization*, 3rd ed. (Wiley, Hoboken, NJ, 2006), p. 781.
[14]S. A. Veldhuis, P. Brinks, T. M. Stawski, O. F. Gobel, and J. E. ten Elshof, J. Sol-Gel Sci. Technol. **71**, 118 (2014).
[15]H. Richter, Z. P. Wang, and L. Ley, Solid State Commun. **39**, 625 (1981).
[16]A. Perez-Rodrıguez, A. Romano-Rodrıguez, R. Cabezas, J. R. Morante, T. Jawhari, and C. E. Hunt, J. Appl. Phys. **80**, 5736 (1996).
[17]D. B. Cuttriss, Bell Syst. Tech. J. **40**, 509 (1961).
[18]S. K. Sahari, H. Murakami, T. Fujioka, T. Bando, A. Ohta, K. Makihara, S. Higashi, and S. Miyazak, Jpn. J. Appl. Phys. **50**, 04DA12 (2011).
[19]A. N. Nazarov, V. M. Pinchuk, T. V. Yanchuk, V. S. Lysenko, Ya. N. Vovk, S. Rangan, S. Ashok, V. Kudoyarova, and E. I. Terukov, Int. J. Hydrogen Energy **26**, 521 (2001).
[20]A. N. Nazarov, V. M. Pinchuk, T. V. Yanchuk, V. S. Lysenko, and S. Ashok, Phys. Rev. B **58**, 3522 (1998).
[21]M. Stavola, *Proceedings of the 5th International Symposium on Advanced Science and Technology of Silicon Materials*, Kona, Hawaii (2008), p. 337.
[22]S. J. Pearton, J. W. Corbett, and M. Stavola, *Hydrogen in Crystalline Semiconductors* (Springer-Verlag, Heidelberg, 1992).
[23]E. Mosconi, D. Meggiolaro, H. Snaith, S. D. Stranks, and F. De Angelis, Energy Environ. Sci. **9**, 3180 (2016).
[24]L. G. Parrat, Phys. Rev. **95**, 359 (1954).
[25]J. S. Pedersen and I. W. Hamley, J. Appl. Cryst. **27**, 36 (1994).